Eur. Phys. J. E **2**, 125–136 (2000)

THE EUROPEAN PHYSICAL JOURNAL E

EDP Sciences

Binding of actin filaments to charged lipid monolayers: Film balance experiments combined with neutron reflectivity

B. Demé[1,a], D. Hess[1], M. Tristl[1], Lay-Theng Lee[2], and E. Sackmann[1]

[1] Technische Universität München, Physik Department, Lehrstuhl für Biophysik E22, James-Franck-Str., D-85747 Garching, Germany
[2] Laboratoire Léon Brillouin, CEA-CNRS, Centre d'Études de Saclay, F-91191 Gif sur Yvette, France

Received 11 August 1999

Abstract. The binding of polymerised actin—a prototype of semi-flexible macromolecule—to lipid monolayers is studied by neutron reflectivity to deduce the average thickness, the interfacial roughness and the polymer volume fraction of the adsorbed film. Electrostatic interaction between actin filaments (F-actin) and the lipid monolayer is mediated through a cationic lipid (1,2-dimyristoyl-3-trimethylammonium-propane, DMTAP). The adsorbed F-actin forms a monolayer with an average thickness of 69 to 84 Å, depending on the ionic strength of the buffer and surface charge density of the monolayer. The volume fraction of F-actin in the adsorbed layer can be as high as 0.29. The thickness and high volume fraction of the actin layer suggest that actin filaments lie flat on the surface and form nematic ordering. The binding-unbinding equilibrium of F-actin is controlled by the ionic strength and exhibits a strong hysteresis. In contrast to the results obtained for filamentous actin, monomeric actin (G-actin) shows no detectable binding to the positively charged lipid layers.

PACS. 61.12.Ha Neutron reflectometry – 68.55.Jk Structure and morphology; thickness

1 Introduction

F-actin is a large and filamentous semi-flexible macromolecule that is often closely connected to cell membranes. A prominent example is the envelope of eukaryotic cells which is a stratified shell composed of a lipid-protein bilayer and a thin shell formed by densely packed and cross-linked actin filaments. These filaments are coupled to the inner leaflet of the bilayer by various coupling proteins also called actin-binding proteins [1,2]. Another example is the densely packed actin-spectrin network of the inner ear cell, which appears to be responsible for the electromechanical oscillatory behaviour of the cells [3]. The elastic properties of the composite shell depend critically on the coupling strength between the two subshells. In general, the coupling is mediated by various families of coupling proteins, which can bind to integral membrane proteins, such as talin in the case of integrin [4]. A more exotic actin-membrane connector is hisactophilin (found in *Dictyostelium* cells) which can link the actin filaments directly to lipid leaflets through a hydrophobic anchor in combination with electrostatic forces. This mode of coupling was first demonstrated by neutron reflectivity studies [5].

In the present study, we have investigated the direct coupling of actin to lipid monolayers by electrostatic forces. This work was motivated by two aims: to design *in vitro* models of the composite cell membranes for systematic studies of the viscoelastic properties of such stratified soft shells, and to further explore the application of neutron reflectivity as a tool to study protein-lipid interactions and protein recognition processes at biofunctionalised surfaces [5–9].

We have studied the electrostatic binding of monomeric and polymerised actin to positively charged monolayers composed of the neutral phospholipid 1,2-dimyristoyl-phosphatidylcholine (DMPC) and the cationic lipid 1,2-dimyristoyl-3-trimethylammonium-propane (DMTAP) as an example of direct actin-membrane interaction. At a *p*H of 7.4, each actin monomer bears an excess of four negative charges ($pI_{\mathrm{actin}} = 5.6$), and the binding of actin filaments can be mediated by the interaction with positively charged monolayers. Changing the DMTAP/DMPC molar ratio can easily vary the surface charge density of the monolayers.

2 Materials and methods

2.1 Buffers and lipids

Two specific buffers were prepared according to the studied actin form (G = globular, F = filamentous). G-buffer

[a] *Permanent address*: Institut Laue-Langevin, B.P. 156, F-38042 Grenoble Cedex 9, France.
e-mail: deme@ill.fr

of *p*H 7.4 (2 mM Tris-HCl, 1 mM ATP) and F-buffer of *p*H 7.4 (2 mM Tris-HCl, 1 mM ATP, 2 mM $MgCl_2$, and KCl from 0 to 1 M) were prepared in Millipore water for fluorescence film balance experiments and in D_2O for neutron reflectivity experiments. Heavy water (99.9% D) was from Euriso-top (Saclay, France).

DMPC (1,2-dimyristoyl-sn-glycero-3-phosphocholine) and DMTAP (1,2-dimyristoyl-3-trimethylammonium propane) were products of Avanti Polar Lipids (Alabaster, AL, USA). They were dissolved in pure chloroform and in 9/1 chloroform/methanol mixtures, respectively. Head group labelled Texas Red-DPPE (1,2-dipalmitoyl-sn-glycero-3-phosphoethanolamine) was from Molecular Probes (Leiden, Netherlands).

2.2 Actin purification

Actin was prepared according to the method of Pardee and Spudich [10], from acetone powder obtained from rabbit back muscle, with an additional gel filtration step as described by MacLean-Fletcher and Pollard [11]. The latter step is essential to remove residual cross-linked polymers [12]. Polymerising activity of the purified actin was tested by falling ball viscosimetry. Its concentration was determined from absorption, using a coefficient of 0.63 (0.1%, 290 nm). G-actin was lyophilised in G-buffer in the presence of sucrose (2 mg/mg protein) and stored at −20 °C. Prior to use, the lyophilised actin was dissolved in pure water, centrifuged for 2 h at 20 000 *g* (4 °C) and dialysed against G-buffer. For the neutron reflectivity experiments, all steps after freeze-drying were performed in D_2O. In this way, change in the scattering length density of the subphase due to injection of light water was avoided. The scattering length density of the subphase was therefore controlled and could be kept constant over several hours by use of a completely closed trough.

2.3 Polymerisation of G-actin

Two distinct procedures have been used to polymerise G-actin. In the first one, actin was polymerised in F-buffer on ice overnight and then injected in the trough. In the second one (*in situ* polymerisation), G-actin was injected as monomer in the trough filled with F-buffer (polymerisation at 20 °C). Injection of F- or G-actin was always preceded by the compression of the lipid layer to avoid unspecific adsorption and denaturation at the air-buffer interface. In a few experiments, polymerised F-actin was stabilised by phalloidin (Sigma, Germany). For the fluorescence microscopy experiments, actin was covalently labelled with NBD-Cl or Rhodamine-NHS (both from Molecular Probes) according to Detmers *et al.* [13] and Okabe and Hirokawa [14], respectively.

2.4 Neutron reflectivity

The physical principle and the applications of neutron reflectivity of soft interfaces have been reviewed by Russell [15] and by Penfold and Thomas [16]. The optical laws of reflection and refraction at interfaces apply also to neutrons. In the absence of absorption, the refractive index for neutrons of wavelength λ is given by

$$n = 1 - \frac{\lambda^2 \rho_c}{2\pi}, \tag{1}$$

where ρ_c is the coherent scattering length density of the material. Using a polychromatic beam of cold neutrons impinging on a surface at fixed grazing angle of incidence θ, total reflection of the beam is observed for any wavelength larger than the critical wavelength λ_c, defined by

$$\lambda_c = \theta \left(\frac{\pi}{\rho_c}\right)^{1/2}. \tag{2}$$

In the *time of flight* technique applied here, the surface is illuminated by a pulsed neutron beam of broad band pass (3–25 Å) at a fixed incident angle. Reflected neutrons exhibit a delay, which is a function of their velocity. The *time of flight* of a neutron is the time elapsed between its emission at the position of the chopper and its detection. The wavelength is obtained according to

$$\lambda = \frac{ht}{mL}, \tag{3}$$

where h is Planck's constant, t the time of flight, m the neutron mass and L the chopper-to-detector distance.

The reflectivity, R, is the ratio of the intensity of the specularly reflected beam (I_r) and that of the incident beam (I_i). For a sharp and structureless interface (Fresnel) where the refractive index varies as a step-like function at the transition from one medium to the other, R is given by

$$R(\lambda) = 1, \quad \text{for } \lambda > \lambda_c, \tag{4a}$$

and

$$R(\lambda) = \left[\frac{1 - [1 - (\lambda/\lambda_c)^2]^{1/2}}{1 + [1 - (\lambda/\lambda_c)^2]^{1/2}}\right]^2, \quad \text{for } \lambda < \lambda_c. \tag{4b}$$

In the presence of a laterally homogeneous thin film intercalated between two infinite half-spaces, the reflectivity is expressed as [17]

$$R(\lambda) = \frac{r_{12}^2 + r_{23}^2 + 2r_{12}r_{23}\cos(2\beta)}{1 + r_{12}^2 r_{23}^2 + 2r_{12}r_{23}\cos(2\beta)}, \tag{5}$$

where r_{ij} the Fresnel coefficient at the ij interface and β are defined as

$$r_{ij} = \frac{n_i \sin\theta_i - n_j \sin\theta_j}{n_i \sin\theta_i + n_j \sin\theta_j}, \tag{6}$$

and

$$\beta = \frac{2\pi}{\lambda} n_2 d_2 \sin\theta_2. \tag{7}$$

The subscripts refer to air (1), the interfacial layer (2) and the substrate (3). d_2 is the thickness of the layer. This

Table 1. Molecular weight, density, molecular volume and scattering length density of the compounds used in this study.

Compound		M $(\mathrm{g \cdot mol^{-1}})$	d $(\mathrm{g \cdot cm^{-3}})$	V $(\mathrm{\AA^3})$	ρ $(\times 10^6\ \mathrm{\AA^{-2}})$
Water	H_2O	18	0.998	30	−0.56
Heavy water	D_2O (99.9% D)	20	1.105	30	6.36
DMPC	$C_{36}H_{72}O_8NP$	677	1.03	1094	0.28
DMTAP	$C_{34}H_{68}O_4N$	554	0.94	980	0.04
DMPC head (dry)	$-C_{10}H_{18}O_8NP$	311	1.54	335	1.79
DMTAP head (dry)	$-C_8H_{14}O_4N$	188	1.68	221	1.80
DMPC/TAP tails	$-C_{26}H_{54}$	366	0.80	759	−0.38
Actin	$C_{1848}H_{2914}O_{563}N_{492}P_{20}$	41644	1.38	50105	1.86
Actin/D_2O[a]	$C_{1848}H_{2485}D_{429}O_{563}N_{492}P_{20}$	42073	1.40	50105	2.93

[a] Accounting for an exchange of 79.5% of labile hydrogen (23).

approach can be extended without too much difficulty to three or four discrete layers. In general, when the profile varies not abruptly but smoothly at the interface, a usual method for calculating the reflectivity is to divide the interface into a finite number of uniform and discrete layers, and to calculate the Fresnel reflectivity at each interface. In this case, one can apply the matrix formalism used in conventional optics to calculate the reflectivity of multilayers where the elements of each layer are represented in a matrix form [17]. Multiplication of all the matrices results in a final two-by-two matrix, the elements of which describe the resulting reflectivity.

In the present study, we used protonated lipids with scattering length densities close to that of air, so that the contrast of the lipid film could be completely matched. The reflectivity of the lipid monolayer spread on a D_2O subphase in the absence of actin could not be distinguished, in the accessible q-range, from the reflectivity of the D_2O subphase alone. Both reflectivities were perfectly fitted by a single Fresnel curve. Matching the lipid contrast to the air allowed to use a single layer model for the analysis of the grafted actin filaments, thus reducing drastically the number of adjustable parameters in the fits. Consequently, the thickness of the adsorbed actin layer, the surface roughness and the volume fraction could be determined with high precision.

2.5 Neutron reflectivity set-up

The intensity distribution of the specularly reflected neutron beam was measured on time-of-flight instruments DESIR and EROS at the Orphée reactor (Laboratoire Léon Brillouin, Centre d'Études de Saclay, France). The characteristics of these two instruments can be found elsewhere [18]. For this experiment, a small teflon trough ($80 \times 40 \times 4\,\mathrm{mm^3}$, $V = 13\,\mathrm{ml}$) was installed in the sample position. The trough was enclosed in a thermostated aluminium box equipped with quartz windows. A platinum Wilhelmy plate was used to control the surface tension of the buffer prior to spreading of the lipid and to monitor the surface pressure of the monolayer. The desired pressure was adjusted by spreading appropriate aliquots of lipid solution at constant area.

Typical durations of data acquisitions were 6 hours on DESIR and 2 hours on EROS. Shorter acquisition times were also used to check time-dependent effects such as adsorption kinetics. When no time dependence of the reflected signal was observed the successive runs were added together to improve the statistics.

After TOF analysis and normalisation to the incident beam intensity, a constant background was subtracted from to the reflectivity data. Pure D_2O was used to determine the precise incident angle, θ, and the angular resolution, $\Delta\theta$, as well as the surface roughness σ. The reflectivity is denoted $R(q_z)$, where q_z, the scattering vector normal to the reflecting surface, is given by $q_z = (4\pi/\lambda)\sin\theta$. The exact angle of incidence θ determined were 1.538 degrees on DESIR, 1.752 degrees on EROS and $\Delta\theta/\theta$ were 0.05 and 0.07, respectively. A roughness of 3 Å was used in the calculation. We checked that the scattering length density and the background were the same for D_2O buffers and pure D_2O. For concentrated KCl buffers the scattering length density of the subphase was corrected by using the scattering length of KCl and tabulated densities of concentrated KCl solutions [19]. This correction gave a good agreement between the calculated Fresnel reflectivity and the experimental curve.

2.6 Scattering length densities

The scattering length densities of the compounds have been calculated according to their chemical structures and densities (Tab. 1). The actin density was calculated from the primary sequence of rabbit skeletal muscle α-actin [20] leading to a molecular weight of 41640, and from the partial specific volumes of amino acid residues [21]. Atomic scattering lengths were taken from Sears [22]. The rate of labile hydrogen exchange of actin was calculated according to a contrast variation experiment by Mendelson and Timmins [23]. The match point obtained at 41.2% D_2O (v/v) corresponds to a deuteration of 79.5% of all

exchangeable hydrogens. In the calculation of the surface excess of F-actin, we have used this result to account for the partial exchange of hydrogen with the solvent. The scattering length density in D_2O is 2.93×10^{-6} Å^{-2} instead of 3.18×10^{-6} Å^{-2} for a theoretical exchange of 100%. The scattering length density of DMTAP given as comparison in Figure 1 shows that this lipid is naturally matched to the air under its fully protonated form.

2.7 Calculation of actin surface excess

Analysis of reflectivity curves gives the mean scattering length density (ρ) and the thickness (L) of the actin layer. The two roughness parameters account for inhomogeneities at the boundaries of the layer. In solution, and for any D_2O composition of the buffer the actin scattering length density may be calculated according to

$$\rho_{\text{actin}} = 1.86 \times 10^{-6} + \Delta\rho\Phi_{D_2O}, \tag{8}$$

$\Delta\rho$ being the scattering length density difference between actin in H_2O and in D_2O, and Φ_{D_2O} the volume fraction of D_2O in the buffer. In dilute protein solutions, the effect of hydrogen exchange on the scattering length density of the solvent can be neglected.

In a layer of adsorbed filaments the mean scattering length density is defined by

$$\langle\rho_{\text{layer}}\rangle = \rho_{\text{buffer}}\Phi_{\text{buffer}} + \rho_{\text{actin}}\Phi_{\text{actin}}, \tag{9}$$

with

$$\Phi_{\text{actin}} = 1 - \Phi_{\text{buffer}}. \tag{10}$$

From (9) and (10), the volume fraction of actin in the layer is calculated according to

$$\Phi_{\text{actin}} = \frac{\rho_{\text{buffer}} - \langle\rho_{\text{layer}}\rangle}{\rho_{\text{buffer}} - \rho_{\text{actin}}}, \tag{11}$$

where $\langle\rho_{\text{layer}}\rangle$ is the only fitted parameter, the other scattering length densities being known or resulting from the sample preparation. Finally, the amount of adsorbed actin is obtained by integrating the concentration profile, giving for a single step function:

$$\Gamma_{\text{actin}} = \Phi_{\text{actin}} d_{\text{actin}} L. \tag{12}$$

2.8 Film balance and fluorescence microscope

The set-up consists of a Zeiss epifluorescence microscope (Axiovert) equipped with filter sets for NBD and Rhodamin/Texas Red fluorescence, an Olympus LWD CD-Plan 40× objective and a Zeiss HBO100 light source [24–26]. The microscope is mounted on an x-y-z translation stage above a Langmuir trough. Images of the fluorescence microscope objective were projected on a SIT-camera (Hamamatsu C2400) connected to a SVHS video

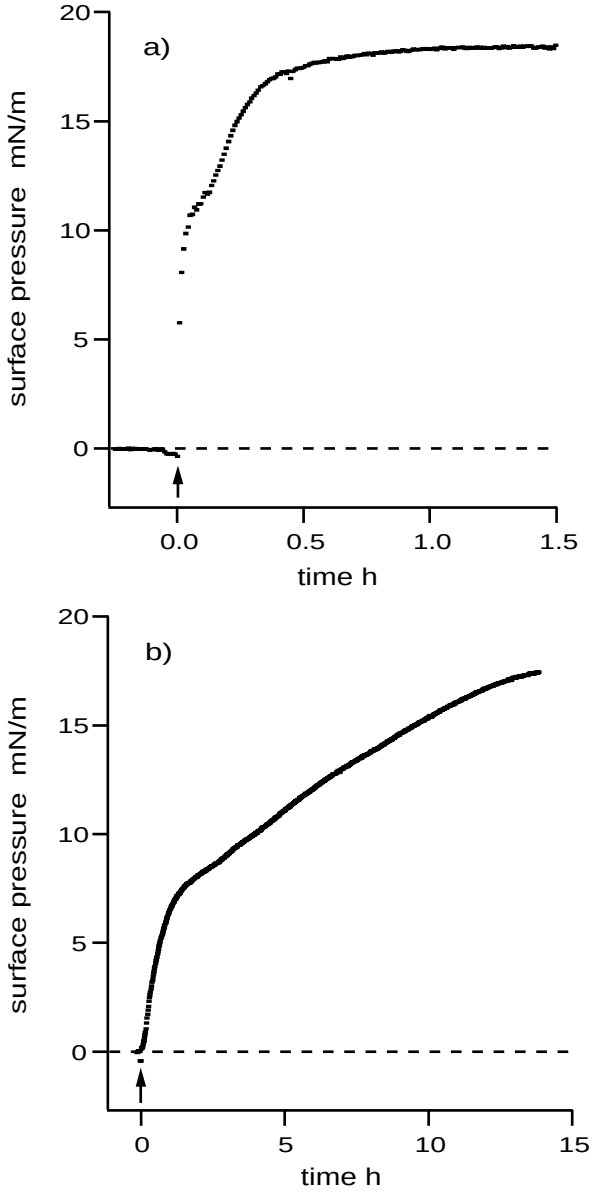

Fig. 1. Adsorption kinetics of F-actin (a) and G-actin (b) at the air-water interface. The method of *in situ* polymerization was used in the case of F-actin.

display. Fluorescence emission spectra and intensities were recorded by an attached spectrometer. The surface pressure of the monolayers was measured with a Wilhelmy plate calibrated by comparison with the lateral pressure of the gel-to-liquid crystalline phase transition of pure arachidic acid at 20 °C (24.5 mN/m). Proteins were added to the subphase through an injection hole in the teflon trough. The temperature was controlled by Peltier elements below the trough (±0.2 °C). By mounting the fluorescence microscope on a motorised x-y-z translation stage the surface can be scanned in the plane of the monolayer by moving the objective in the x and y directions. The z-translation of the microscope is used to scan the fluorescence along the normal of the monolayer. In this way, the distribution of fluorescently labelled proteins at the

interface and in the bulk (fluorescence intensity profiles) can be measured by recording the fluorescence intensity as a function of z. The x, y and z resolutions obtained with this set-up make it very complementary to the technique of specular neutron reflectivity.

3 Results

3.1 Adsorption kinetics of G- and F-actin at the air-water interface

We investigated the time-dependent adsorption of actin at the air-water interface and the saturation behaviour of the adsorption process by film balance experiments (Fig. 1). A solution of G-actin was injected in the trough containing a non-polymerising (G-) or polymerising (F-) buffer. The formation of the adsorbed film was followed by the pressure increase. The kinetics of monomeric and polymerised actin are very different. Filamentous (F-) actin adsorbs much faster than globular (G-) actin at the air-water interface. The time required to reach the equilibrium surface pressure is one hour in the case of F-actin and more than 10 hours for G-actin. But the adsorption process of both forms of actin also shows common features. Firstly, they exhibit a two-step adsorption kinetic: A fast adsorption step completed after several minutes followed by a second one, much slower. In this second process, the equilibrium is reached within one hour (F-actin) and several hours (G-actin). The second common feature is the equilibrium pressure of the two protein layers, which is very close: 17.5 mN/m for G-actin and 18.4 mN/m for F-actin. These values can be considered as the spreading pressure of the protein in the two states. The shoulder observed above 10 mN/m a few minutes after injection is reproducible and is attributed to the beginning of the denaturation of the protein exposed to the air. The slow increase in pressure observed for G-actin is attributed to the aggregation of denatured G-actin, which was observed previously by rheological measurements.

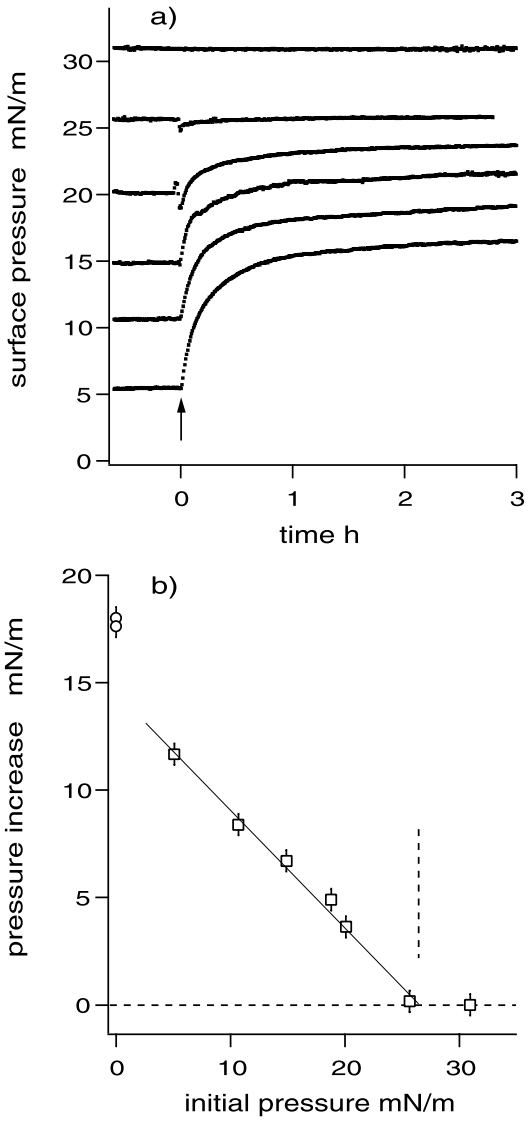

Fig. 2. (a) Adsorption kinetic of F-actin at the DMPC-buffer interface at various initial DMPC surface pressures by the method of *in situ* polymerization. The arrow indicates the injection of G-actin in the trough filled with F-buffer. (b) Spreading pressure of F-actin (○) and surface pressure increase at steady state (□) upon adsorption of F-actin at the DMPC-buffer interface. The pressure increase is calculated from a) according to $\Delta\Pi = \Pi_{\mathrm{DMPC/F\text{-}actin}} - \Pi_{\mathrm{DMPC}}$.

3.2 Adsorption of F-actin to neutral DMPC monolayers

3.2.1 Film balance experiments

The adsorption kinetic of F-actin formed by *in situ* polymerisation at the DMPC-buffer interface is shown in Figure 2 for various initial surface pressures of the monolayer. The initial pressure of the film was adjusted to the desired value and the experiment was performed at constant area. After the relaxation of the monolayer had been completed (0.5 to 1 mN/m), the protein was injected and the pressure was recorded until saturation was observed.

In the presence of a lipid monolayer only one adsorption step was observed for all initial surface pressures of the studied monolayers. This suggests that in the presence of a lipid monolayer protein denaturation is prevented even at low surface pressures of a few mN/m. This is in agreement with previous studies [27].

The increase in surface pressure ($\Delta\Pi$) as a function of the initial pressure of the DMPC monolayer is shown in Figure 2. Two distinct regimes are clearly visible: a low-pressure regime where F-actin adsorbs to the monolayer leading to a pronounced pressure increase, and a high-pressure regime where no change in the pressure takes place. The spreading pressure of F-actin (opened circles) is given for comparison.

These observations indicate that in the absence of electrostatic interaction or specific binding between the

filaments and the monolayer, non-specific adsorption of actin is inhibited only if the initial pressure of the monolayer is much larger than the spreading pressure of the protein. The surface pressure required to avoid non-specific adsorption ($\Pi > 26.5\,\mathrm{mN/m}$) is significantly higher than the spreading pressure of F-actin (18.4 mN/m). The transition between the two regimes defines the minimum pressure of the lipid layer required to investigate specific binding of the filaments. Since the transition pressure can depend on the actin concentration, it is essential to know that pressure for the following experiments with the charged lipid. For this reason all binding experiments were performed at the same actin concentration and well above the spreading pressure of actin, typically between 30 and 35 mN/m.

3.2.2 Neutron reflectivity

Neutron reflectivity experiments with neutral DMPC monolayers showed that upon injection of actin filaments, a slight deviation from the lipid reflectivity was observed. The decrease of the reflectivity is consistent with a hydrogen enrichment at the interface due to the replacement of D_2O molecules by protonated actin filaments, but this deviation is too low to be reliably fitted and to obtain quantitative structural data.

3.3 Binding of F-actin to positively charged monolayers

3.3.1 Reflectivity from buffer and DMTAP monolayer matched to air

Table 1 shows that the mean scattering length density of DMTAP (0.04×10^{-6} Å^{-2}) is very close to that of air. The size of the small headgroup consisting of a quaternary ammonium group is below the resolution of the instrument. Thus, in the accessible q_z range, the DMTAP layer is perfectly matched to air. This simplifies the data analysis by reducing the number of parameters to be fitted. The reflectivity curves obtained with the D_2O F-buffer and a DMTAP monolayer compressed to 35 mN/m are given in Figure 3. The buffer and the lipid reflectivity are, as expected, in very good agreement with the Fresnel curve.

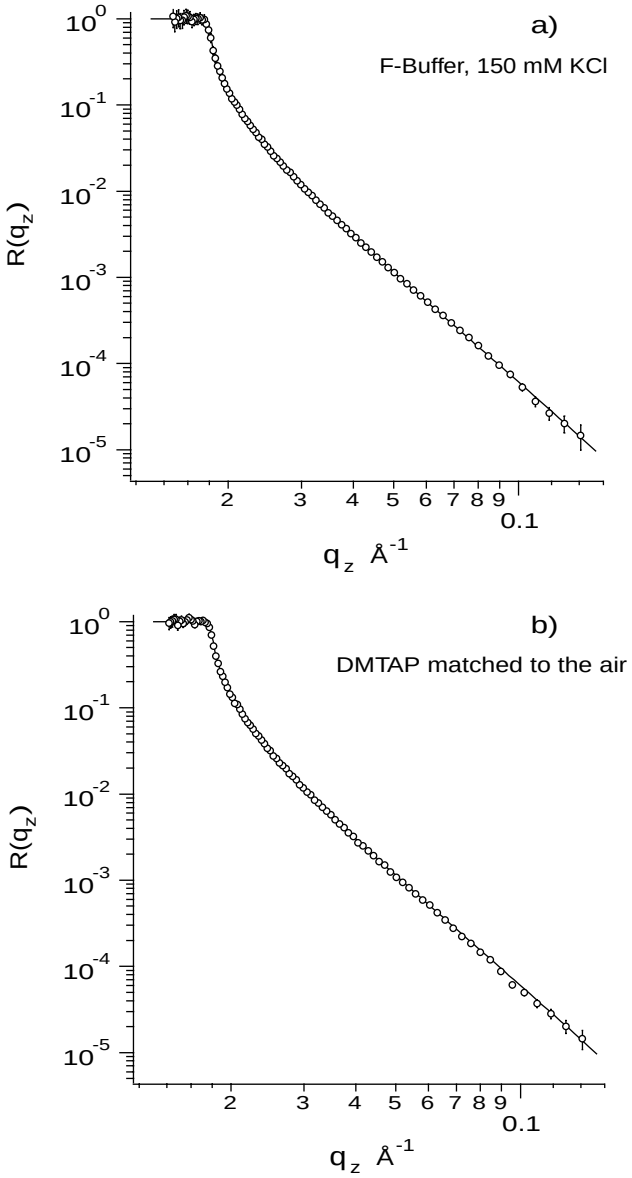

Fig. 3. Reflectivity curves of pure D_2O F-buffer (a) and in the presence of a DMTAP layer matched to the air at $\Pi = 35\,\mathrm{mN/m}$ (b). The solid line is the Fresnel curve calculated with a scattering length density $\rho = 6.36 \times 10^{-6}$ Å^{-2} and a roughness $r = 3$ Å. The angle of incidence (1.752°) and the beam divergence ($\Delta\theta/\theta = 0.07$) are taken into account in the calculation.

3.3.2 Reflectivity from F-actin adsorbed to DMTAP layers

Reflectivity experiments have been performed using a protonated DMTAP layer matched to the air and spread on a D_2O buffer. Figure 4 shows the reflectivity curves ($R(q_z) \cdot {q_z}^4 = f(q_z)$ plots) obtained for actin layers bound to the DMTAP monolayer on a D_2O buffer in the presence of an interfacial film. This representation enhances the deviation to the ${q_z}^{-4}$ decay due to the sharp interface. The curves correspond to increasing salt concentrations: 0, 10, 50 and 150 mM KCl. The lipid layer was compressed to 35 mN/m before the injection of actin, which was polymerised *in situ*. Results obtained with the two different procedures are given in Table 2. The F-actin surface excesses have been calculated by integrating the step-like density profile according to equation (12). The values reported in Table 2 show that with increasing ionic strength the thickness of the layer increases while the actin volume fraction decreases. In the range 0–150 mM KCl, the effect of these structural changes on the surface excess (Γ) is a decrease from 2.5 to 2.1 mg/m^2 in the *in situ* polymerisation, while the decrease observed with pre-polymerised

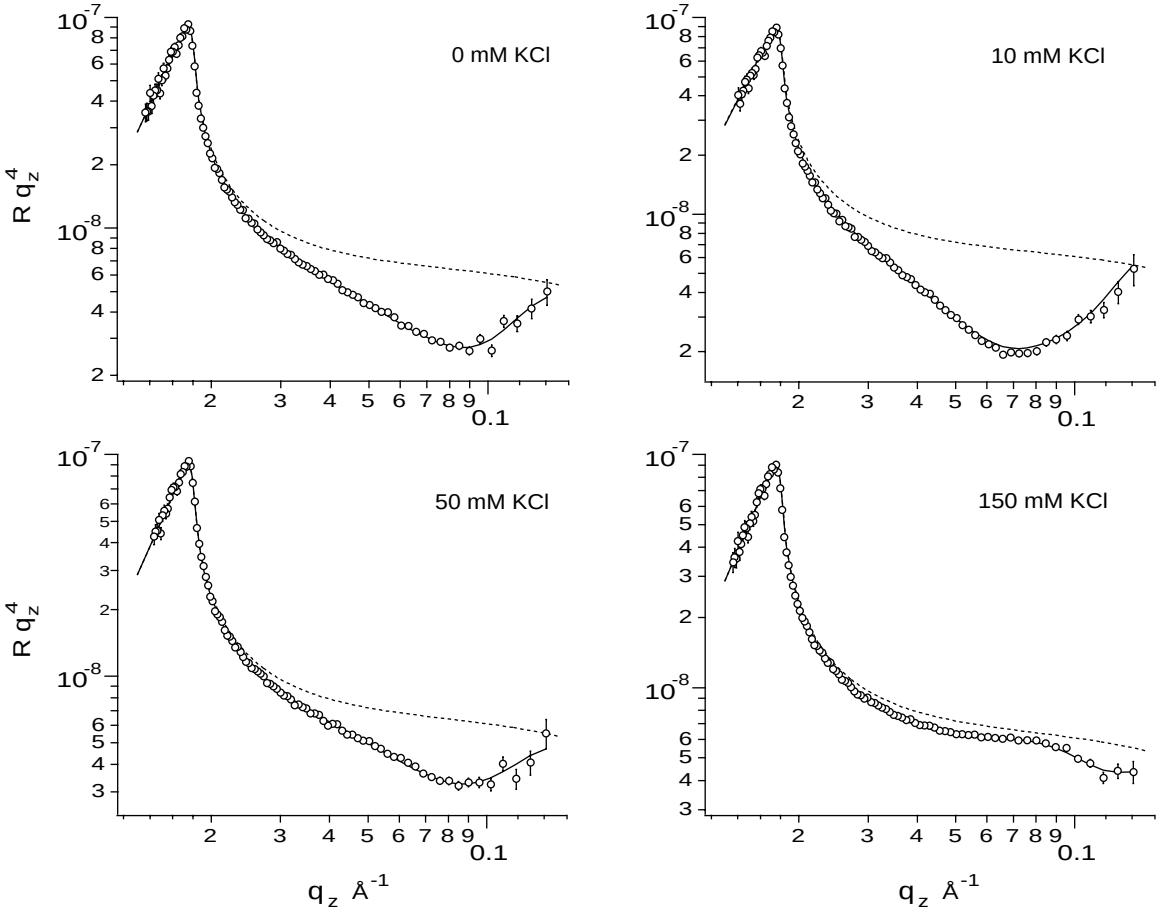

Fig. 4. Reflectivity curves ($R(q_z) \cdot {q_z}^4 = f(q_z)$ plots) of F-actin layers bound to fully charged monolayers (100% DMTAP) at various salt concentrations. The solid lines are the best fits using a single-layer step profile and the dash lines the respective Fresnel curves accounting for the salt concentration (KCl) of the buffer.

filaments is less pronounced. The decrease in actin volume fraction in the layer with no significant change of Γ can be interpreted as a relaxation of the bound actin upon salt addition. A significant inhibition of the actin binding is observed at 1 M KCl.

3.3.3 Unbinding of the filaments by salt addition

We have investigated the unbinding of actin by adding salt to the subphase after an F-actin layer had been adsorbed in a low ionic strength buffer (2 mM Tris, 1 mM ATP). After measuring the reflectivity of the adsorbed protein layer, the KCl concentration in the subphase was increased by injection of a concentrated KCl solution. The reflectivity was recorded after each injection. The surface excesses obtained from the two experiments i) inhibition of adsorption due to the presence of KCl, and ii) unbinding of adsorbed filaments by addition of KCl, are plotted in Figure 5. The two different methods of controlling the electrostatic adsorption of actin to cationic lipid layers show a strong hysteresis. A high salt concentration (1 M) is required to observe a significant unbinding of the filaments (0.6 mg/m^2) adsorbed at low ionic strength (2.5 mg/m^2). In contrast, when the salt is present before binding of the filaments, there is a significant inhibitory effect by 10 mM KCl on the adsorption of actin (1.3 mg/m^2). In the adsorption-inhibition experiment, a concentration of 150 mM KCl reduces the surface excess to the same value as 1 M KCl added in the unbinding experiment (0.7 mg/m^2). However, even at this high ionic strength, there are still filaments bound to the interface.

3.3.4 Effect of the surface charge density of the monolayer on actin adsorption

The effect of the monolayer surface charge density on the adsorption of F-actin has been investigated by diluting the charged lipid with neutral DMPC. The surface charge density was varied from pure DMTAP to mixtures containing 10 and 1 mol% of cationic lipid. The results are given in Table 3. At high surface pressures corresponding to a solid phase, the area per charge is in the range 40–50 Å^{-2} for the pure DMTAP layer and 4000–5000 Å^2 for the 1% DMTAP monolayer. Considering the actin surface excess and a net charge of -4 per actin monomer at *p*H 7.4, we have calculated the ratio of charges per unit

Table 2. Comparison of the structure of F-actin layers bound according to the two different procedures, 1) *in situ* polymerisation, and 2) overnight pre-polymerisation on ice. The scattering length density of the layer (ρ), the thickness (L) and the two roughnesses (r_1 and r_2) are the fitted parameters. The volume fraction of actin in the layer (Φ) and the surface excess (Γ) are calculated according to equations (11) and (12), respectively.

Method	KCl (mM)	ρ ($\times 10^6$ Å^{-2})	L (Å)	r_1 (Å)	r_2 (Å)	Φ_{actin}	Γ_{actin} (mg/m^2)
1	0	5.34	69	5	< 1	0.26	2.5
	150	5.46	74	8	< 1	0.23	2.3
	500	5.56	79	2	4	0.19	2.1
	1000	5.85	63	3	< 1	0.08	0.7
2	0	5.45	66	< 1	< 1	0.21	1.9
	150	5.41	71	< 1	< 1	0.21	2.0
	500	5.55	84	< 1	< 1	0.15	1.8

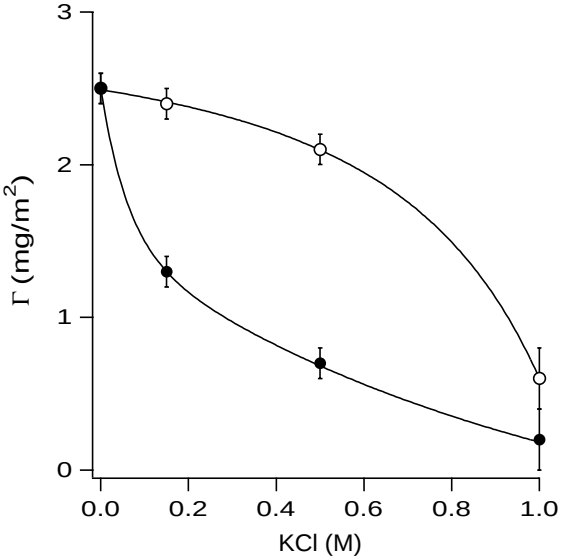

Fig. 5. Surface excess of F-actin bound to fully charged DMTAP layers as a function of salt concentration in the buffer. Open circles correspond to the unbinding of the filaments induced by successive injections of concentrated salt in the trough (unbinding experiment). Filled circles correspond to separate binding experiments started at various salt concentrations (inhibition experiment).

area in the lipid layer and in the bound protein layer. This ratio indicates whether the monolayer bears an excess of (+) charges relative to the protein layer. From Table 3, it is interesting to note that as long as the monolayer bears an excess of charges (100% and 10% of DMTAP), the volume fraction of actin in the layer and the total amount of adsorbed actin do not change. With 1% of DMTAP in the monolayer, the charge ratio becomes inferior to 1, and the volume fraction and adsorbed amount of actin drop significantly from 0.26 to 0.14, and from 2.5 mg/m^2 to 1.5 mg/m^2, respectively. The thickness of the layer increases from 69 to 78 Å upon dilution of the charges by a factor 100, indicating a weaker interaction between the filaments and the monolayer. This effect is very similar to the screening of the electrostatic interaction by salt.

3.3.5 Depletion of G-actin from positively charged monolayers

Except in the presence of depolymerisation inhibitors such as phalloidin, F-actin solutions contain a non-negligible amount of free G-actin monomers in equilibrium with the filaments [28]. The so-called treadmilling process of polymerisation is responsible for this equilibrium. In order to show that the thin layers observed by neutron reflectivity consist of actin filaments and not of adsorbed monomers, we investigated the adsorption of monomeric actin in G-buffer. In these conditions, no deviation from the Fresnel curve was observed. The fluorescence film balance experiments with NBD-labelled G-actin gave the same result. The behaviour of NBD-G-actin was evaluated by recording the fluorescence intensity while the objective was moved in the vertical direction. This method can detect very low surface excesses of labelled compounds. With its high sensitivity but poor resolution in the direction normal to the interface, the scanning fluorescence technique is an attractive and most complementary method to neutron reflectivity.

As previously with F-actin, the experiment was performed at *p*H 7.4 where actin bears a net charge of -4/monomer, and at the isoelectrical point of actin (5.7). Figure 6 shows fluorescence images of the lipid layer labelled with Texas Red-DPPE and that of NBD-labelled actin. The lipid layer consisted of a mixture of DMPC and DMTAP (80/20 mol/mol) labelled with 0.1% Texas Red-DPPE. The fluorescence images correspond to: A) the background intensity in the absence of lipid and protein, B) the lipid layer in the fluid state at $\Pi = 0.5$ mN/m (same image at the two *p*H); C) the lipid fluorescence during the compression step at *p*H 7.5 and $\Pi = 14$ mN/m, characterised by the appearance of crystalline domains; D) same layer at rest after injection of NBD-G-actin, $\Pi = 21$ mN/m, E) lipid layer fluorescence at rest and *p*H 5.7 ($\Pi = 20$ mN/m) after injection of NBD-G-actin;

Table 3. Effect of the lipid surface charge density and of the lipid/actin charge ratio on the structure and surface excess of adsorbed actin.

DMTAP (mol%)	Area/Charge[a] ($Å^2$)	L (Å)	Φ_{actin} (% v)	Γ_{actin} (mg/m^2)	Area/Actin monomer ($Å^2$)	Monolayer charge excess[b]
100	40	69	0.26	2.5	2800	17.5
10	400	71	0.26	2.5	2800	1.7
1	4000	78	0.14	1.5	4600	0.3

[a] Assuming an average area of 40 $Å^2$ per lipid.

[b] (DMTAP charge density)/(actin charge density) assuming 1 charge per lipid head and 4 charges/actin monomer.

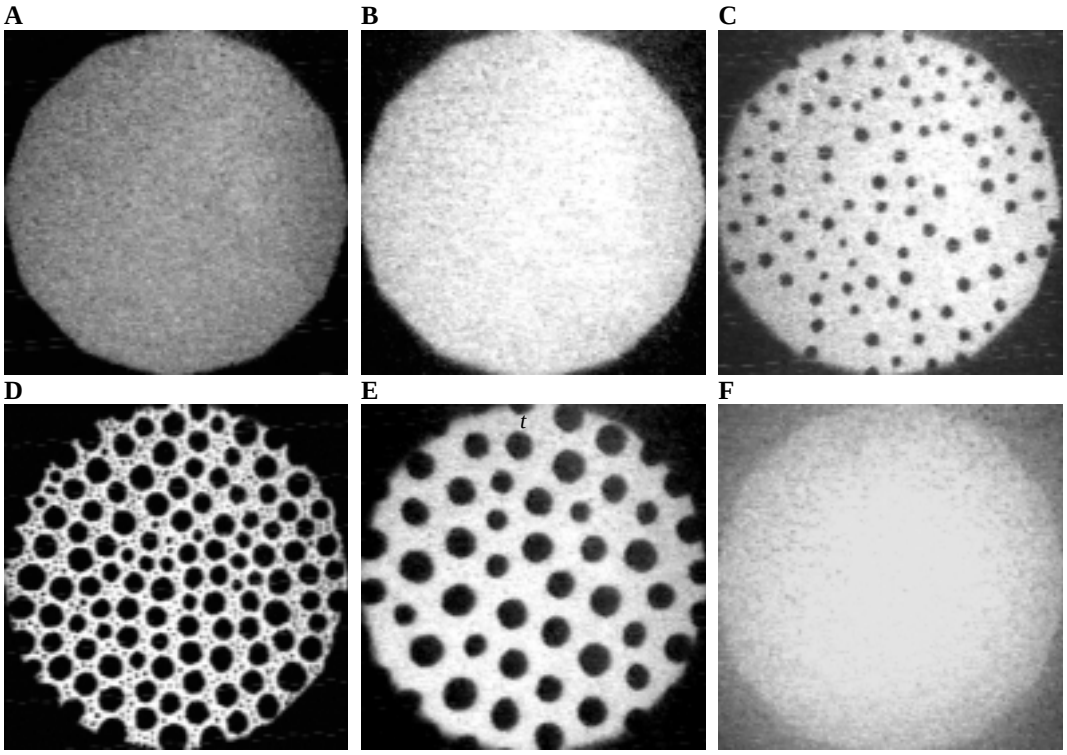

Fig. 6. Fluorescence micrographs of the lipid monolayer (DMPC/DMTAP: 80/20) labelled with 0.1% Texas Red-DPPE and of G-actin labelled with NBD. A) background intensity in the absence of lipid and protein, B) Texas Red fluorescence of a lipid layer in the fluid state at $\Pi = 0.5$ mN/m and *p*H 7.4; C) same layer during compression at $\Pi = 14$ mN/m; D) same layer at rest ($\Pi = 21$ mN/m) after injection of NBD-G-actin, E) lipid layer fluorescence at rest and *p*H 5.7 ($\Pi = 20$ mN/m) after injection of NBD-G-actin; F) NBD fluorescence at *p*H 5.7 adjusted at the focus ($z = 0$) with the Texas Red fluorescence of the lipid layer. In the case of image F it is impossible to focus on the interface, due to the high background fluorescence of the protein in the subphase. The same over-illuminated picture due to the intense subphase fluorescence was observed at the two *p*H.

and F) NBD-actin fluorescence at *p*H 5.7 adjusted at the focus ($z = 0$) with the Texas Red fluorescence from the lipid layer. The unfocussed image 6F is due to the high background fluorescence of the protein in the subphase. The same over-illuminated picture due to the intense subphase fluorescence was observed at both *p*H. The intensity profiles corresponding to images D, E and F (plus that measured at *p*H 7.5, micrograph not shown) are given in Figure 7. The z-scans correspond to the adsorption at *p*H 7.5 (a) and at the isoelectrical point (b). At both *p*H, the lipid fluorescence can be fitted by a single Lorentzian as expected for a thin labelled interfacial layer [24]. The actin fluorescence has been fitted by an Arctangent function, which describes the intensity profile when the labelled species is depleted from the interface [24,25]. The absence of any additional fluorescence peak at the z-position of the interface indicates that there is no binding of actin monomer at the interface.

The addition of phalloidin is a common method to prevent the dissociation of monomers from the polymer chain at actin concentrations below the critical monomer concentration [29]. Comparison of results obtained with

unstabilised and phalloidin-stabilised actin filaments did not show any significant differences. Taken together, these results indicate that no actin in its monomeric form adsorbs to the positively charged lipid layer.

4 Discussion

We have used two different methods to bind actin filaments to charged lipid layers: prepolymerised and *in situ* polymerised filaments. The neutron reflectivity results confirm that both methods are reliable and give similar results. However, as previously evidenced by Taylor and Taylor [29], we have obtained more dense layers using the *in situ* polymerisation of G-actin (Tab. 2). The polymerisation of actin in the subphase yields a better packing than the injection of pre-polymerised filaments. This was verified for several salt concentrations ranging from 0 to 500 mM KCl. Since the *in situ* procedure is rather simple compared to the overnight pre-polymerisation, we have applied it in these experiments. The fact that monomeric G-actin polymerises in the trough and adsorbs at the same time does not affect the final state of the bound F-actin layer. But it is clear from the experiments done in G-buffer that actin has to be in the form of polymerised filaments to adsorb to positively charged monolayers. This is in contradiction with the results of Laliberte and Gicquaud [30] who observed a polymerisation on positively charged vesicles (phosphatidylcholine and stearylamine 90/10), although the experiments were done in depolymerising buffer. However, our results are consistent with those of Taylor and Taylor who observed that quaternary ammonium surfactants are better promoter of 2-D crystal growth than stearylamine.

The formation of F-actin paracrystals on positively charged vesicles and monolayers was observed by Rioux and Gicquaud [31] and Ward *et al.* [32], respectively. The results presented here do not show evidence of existence of paracrystals, but the high filament density, the thickness of the actin layer and its regularity are in good agreement with previous results obtained by optical techniques. For instance, Taylor and Taylor [29] measured a filament spacing in paracrystals of F-actin around 70 Å. In a paracrystal, the spacing of the filaments corresponds to the closest packing. If one considers that this spacing is related to the filament diameter, the thickness of the F-actin layer corresponds to the diameter of a single filament.

In order to propose a model for the adsorbed actin filaments, we have calculated the volume fraction of actin in a monolayer of perfectly aligned filaments. We take the layer thickness of 70 Å measured by neutron reflectivity and fill it with infinite cylinders of cross-section diameter 70 Å. According to the helical structure of F-actin with 13 molecules per 6 turns and a repeat distance of 360 Å [33], one obtains a mass per repeat unit along the filament axis of $13 \times 41640 = 541320\,\mathrm{g \cdot mol^{-1}}$ or 9×10^{-19} g. According to the density of actin ($1.38\,\mathrm{g \cdot cm^{-3}}$), this mass corresponds to an excluded volume of 6.5×10^5 Å^3. Considering the volume of a cylinder with the same length, we obtain a volume fraction of actin of 0.47 in the cylinder. Stacking the cylinders in a flat monolayer reduces the volume fraction by a factor $\pi/4$ in the layer. The resulting volume fraction of actin in the layer is then $0.47 \times \pi/4 = 0.37$. The highest actin volume fraction we have measured is 0.29 at low ionic strength. The value remains below that expected for a perfect packing. With a filament spacing of 90 Å and a thickness of 70 Å, this simple nematic packing model gives the experimental volume fraction of 0.29. This indicates that the high volume fractions we have measured are consistent with the known cross-section of the filaments. The measurements of the volume fraction and thickness of the actin layer can be used to estimate the filament spacing in the 2D-nematic phase of filaments.

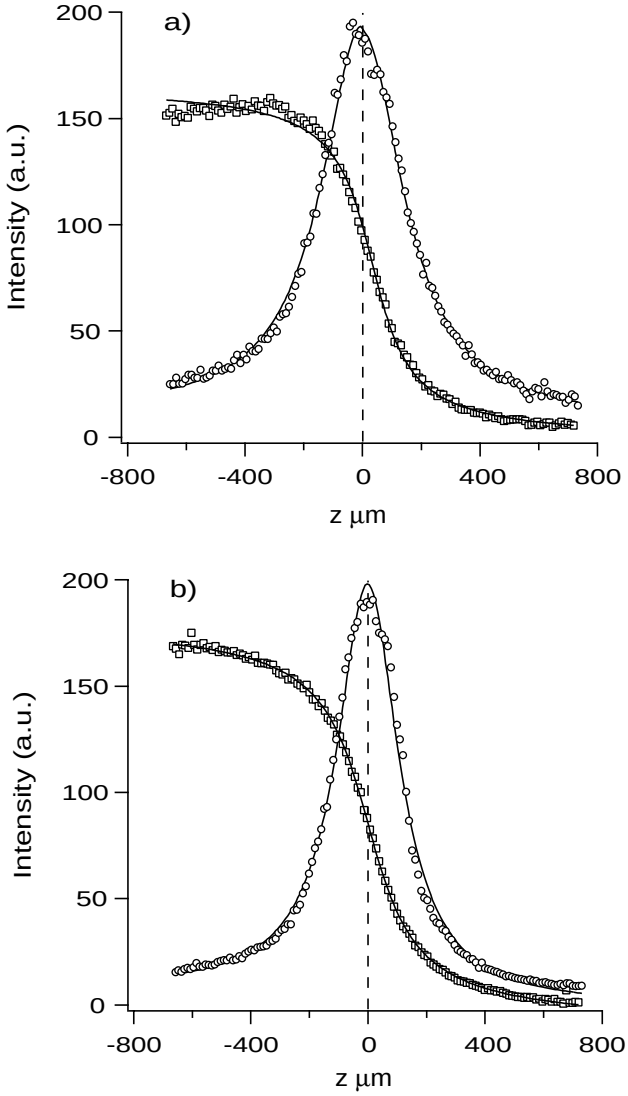

Fig. 7. a) Texas Red and NBD fluorescence intensity profiles corresponding to images 6D and 6E (isoelectric point, *p*H 5.7). b) Same as a) at *p*H 7.4. In both cases the lipid and protein fluorescences are described by an arctan and Lorentzian function, respectively.

Considering the dimensions of G-actin $67 \times 40 \times 37$ Å^3 [28], a 70 Å thick layer could in principle be obtained with adsorbed monomers. However, results show that the layers are constituted of filaments. First of all, the F-actin layer thickness has been measured between 70 Å (in the absence of added salt with *in situ* polymerised filaments) and 84 Å (pre-polymerised filaments after injection of 500 mM KCl). This latter thickness is not compatible with a monolayer of actin monomers. Furthermore, neutron reflectivity and fluorescence microscopy show that G-actin is depleted from the positively charged layers. Finally, no effect of a stabilisation by phalloidin has been observed, indicating that free monomers of G-actin do not compete with filaments for adsorption to the monolayer.

Varying the charge density in the monolayer shows that the amount of adsorbed actin is related to the excess of charges at the interface. The binding of actin decreases when the fraction of charged lipid is reduced below 10%. Above this value, the surface excess of actin is constant and corresponds to the maximum filament density in the presence of excess charges in the monolayer. The electrostatic binding of actin to the lipid layer is attenuated by an increase in ionic strength. The extent of the attenuation depends on whether the process is salt-induced unbinding or inhibition of binding by salt. Thus a strong hysterisis is observed.

At high pressures it is known that DMTAP/DMPC mixtures (like many other mixtures of lipids differing in chain or head group composition) phase separate. This is true for DMTAP/DMPC mixtures whatever the amount of DMTAP in the layer. Solid domains from which the fluorescent probe is excluded, are in coexistence with a continuous fluid phase (Fig. 6). However, in the particular contrast studied here, well-defined domains are contrast matched to the air and to the continuous phase because of the very low contrast between the two protonated lipids. The contrast is only related to the scattering length density difference between TAP and PC heads, the chains having rigorously the same scattering length density. There is then no in-plane contrast in the lipid layer. Furthermore, fluorescence experiments show that there is no selective binding of F-actin to one of the two phases. The low roughnesses derived from the fits are an indication of the smoothness of the layers which is related to their homogeneity.

5 Conclusion

The most pertinent results of the present work may be summarised as follows:

1) At low ionic strength, the maximum surface concentration of actin adsorbed to cationic lipid layers corresponds to a volume fraction of 0.29. This corresponds to 78% of the theoretical packing of perfectly aligned actin rods ($\Phi = 0.37$). Since the thickness of the actin film ($\sim$ 70 Å) agrees well with the filament cross-section diameter, actin filaments are expected to form a parallel nematic liquid crystal-like array.

2) The thickness of the adsorbed actin film (69–84 Å) depends on the salt concentration and surface charge density of the lipid monolayer. Screening the charges by adding salt to the subphase or reducing the surface charge density of the monolayer lead to very similar effects. The actin volume fraction decreases only slightly (from 0.29 to 0.25) by increasing the ionic strength to physiological concentrations ($\sim$ 150 mM) and is only strongly reduced above 500 mM of KCl. The electrostatically controlled binding-unbinding equilibrium exhibits a pronounced hysteresis.

BD is grateful to Prof. E. Sackmann and to his group for their welcome to the Munich laboratory and to the Alexander von Humboldt Foundation for financial support under the form of a grant.

References

1. M. Schleicher, B. André, C. Andréoli, L. Eichinger, M. Haugwitz, A. Hofmann, J. Karakesisoglou, M. Stöckelhuber, A.A. Noegel, FEBS Lett. **369**, 38 (1995).
2. A. Bausch, F. Ziemann, A. Boulbitch, K. Jacobson, E. Sackmann, Biophys. J. **75**, 2038 (1998).
3. T. Arima, A. Kuraoka, R. Toriya, Y. Shibata, T. Uemura, Cell Tissue **263**, 91 (1991).
4. W.H. Goldmann, S. Kaufmann, G. Isenberg, J. Muscle Res. Cell Motility **12**, 492 (1991).
5. C. Naumann, C. Dietrich, A. Behrisch, T. Bayerl, M. Schleicher, D. Bucknall, E. Sackmann, Biophys. J. **71**, 811 (1996).
6. J. Raedler, E. Sackmann, Cur. Op. Solid State Mater. Sci. **2**, 330 (1997).
7. S.J. Johnson, T.M. Bayerl, W. Weihan, H. Noack, J. Penfold, D. Kanellas, A.R. Rennie, E. Sackmann., Biophys. J. **60**, 1017 (1991).
8. M. Lösche, M. Piepenstock, A. Diederich, T. Grünewald, K. Kjaer, D. Vaknin, Biophys. J. **65**, 2160 (1993).
9. D. Vaknin, J. Als-Nielsen, M. Piepenstock, M. Lösche, Biophys. J. **60**, 1545 (1991).
10. J.D. Pardee, J.A. Spudich, Methods Enzymol., **85** 164 (1982).
11. S. MacLean-Fletcher, T.D. Pollard, Biochem. Biophys. Res. Commun. **96**, 18 (1980).
12. F. Schmidt, F. Ziemann, E. Sackmann, Eur. Biophys. J. **24**, 348 (1996).
13. P. Detmers, A. Weber, M. Elzinga, R.E. Stephens, J. Biol. Chem. **256**, 99 (1981).
14. S. Okabe, N. Hirokawa, J. Cell Biol. **109**, 1581 (1989).
15. T.P. Russell, Mater. Sci. Rep. **5**, 171 (1990).
16. J. Penfold, R.K. Thomas, J. Phys. Condens. Matter **2**, 1369 (1990).
17. M. Born, E. Wolf, in *Principles of Optics* (Pergamon Press, Oxford, 1975).
18. `http://www-llb.cea.fr/`
19. D.R. Lide (Editor), in *Handbook of Chemistry and Physics*, 78th edn. (CRC Press, New York, 1997).
20. M. Elzinga, J.H. Collins, W.M. Kuehl, R.S. Adelstein, Proc. Nat. Acad. Sci. **70**, 2687 (1973).
21. A.A. Zamyatin, Prog. Biophys. Mol. Biol. **24**, 107 (1972).

22. V.F. Sears, Neutron News **3**, 26 (1993).
23. R. Mendelson, P. Timmins (private communication).
24. C. Dietrich, W.H. Goldmann, E. Sackmann, G. Isenberg, FEBS Lett. **324**, 37 (1993).
25. S.P. Heyn, R.W. Tillmann, J. Biochem. Biophys. Methods **22**, 145 (1990).
26. A. Behrisch, C. Dietrich, A.A. Noegel, M. Schleicher, E. Sackmann, Biochemistry **34**, 15182 (1995).
27. O. Müller, H.E. Gaub, M. Bärmann, E. Sackmann, Macromelecules **24**, 3111 (1991).
28. P. Sheterline, J. Clayton, J. Sparrow, Protein Profile **2**, 1 (1995) and references cited therein.
29. K.A. Taylor, D.W. Taylor, J. Struct. Biol. **108**, 140 (1992).
30. A. Laliberte, C. Gicquaud, J. Cell Biol. **106**, 1221 (1988).
31. L. Rioux, C. Gicquaud, J. Ultrastruc. Res. **93**, 42 (1985).
32. R.J. Ward, J.-F. Menetret, F. Pattus, K. Leonard, J. Electron Microsc. **14**, 335 (1990).
33. K.C. Holmes, D. Popp, D. Gebhard, W. Kabsch, Nature **347**, 44 (1990).